Balmer emission induced by proton impact on atomic hydrogen

Balmer emission induced by proton impact on atomic hydrogen

I. B. Abdurakhmanov, O. Erkilic, A. S. Kadyrov, and I. Bray
Curtin Institute for Computation and Department of Physics and Astronomy, Curtin University, GPO Box U1987, Perth 6845, Australia

S. K. Avazbaev
Tashkent State Pedagogical University, 27 Bunyodkor Street, Tashkent 100070, Uzbekistan

A. M. Mukhamedzhanov
Cyclotron Institute, Texas A&M University, College Station, Texas 77843, USA

(Dated: April 2, 2019)

The semiclassical two-centre convergent close-coupling approach is applied to study Balmer emission in proton-hydrogen scattering at the incident proton energies from 5 keV to 1 MeV. The approach uses wave-packet pseudostates for the discretization of the continuous spectrum of the hydrogen atom, constructed from the Coulomb wave function. All cross sections for target excitation into the final states with principal quantum numbers $n = 3$ and 4 required for obtaining the Balmer emission cross sections, polarization fraction and Balmer decrement are calculated. Corresponding electron-capture cross sections are also given. A substantial variation in the cross sections for population of magnetic sublevels obtained in different theoretical approaches is found. The present cross section for excitation of the $n = 3$ shell as a whole does not agree with experiment, but supports earlier calculations. At the same time, the individual cross section for excitation of the $3p$ state displays excellent agreement with available experimental measurements. The results for polarisation fraction of the Balmer-α emission significantly disagree with experimental measurements at high energies. The calculated Balmer decrement plateaus at about 100 keV and can be used in astrophysical applications.

I. INTRODUCTION

Collisional excitation of hydrogen plays an important role in fast astrophysical shocks. Modeling these astrophysical processes require the Balmer emission cross section. Particularly, a category of shocks known as Balmer-dominated shocks are driven by astrophysical pistons such as supernova remnants, pulsar wind nebulae, novae, etc. They have an effect on ambient interstellar medium and produce hydrogen lines observed in the Lyman and Balmer series [1]. Moreover, polarized Balmer line emission from supernova remnants can give information about accelerating cosmic rays [2]. Both excitation and charge transfer take place in these Balmer-dominated shocks which can also be relevant in young high-redshift galaxies [3]. The ratio of the Hα to Hβ line intensities (emission cross sections), known as the Balmer decrement, serves as a diagnostic for dust extinction and shock velocities as it is insensitive to electron temperature and density [4, 5]. At relative velocities of $\sim$1000 km/s ($\sim$0.5 a.u.) between colliding particles or larger, the excitation of hydrogen atoms is dominated by the collisions with protons rather than electrons [6]. Therefore, when calculating the cross sections for Balmer-dominated shocks, there are several distinct cases to consider. At low velocities, collisions between protons and hydrogen atoms cause large deflections of the interacting particles and the electron wave function deforms adiabatically and the dominant process is the charge transfer between the colliding particles. In this case, the collision process must be treated in a way that reflects the interaction between various quantum states of the electronic wavefunction. In the higher energy region, the process can be described using Born-type approximations where the proton is considered a small perturbation for the electronic wave function. In this energy region, excitation or ionisation is the dominant outcome of the collisions. At intermediate velocities, the collisional times are of the order of the atomic time-scale. For this reason, a perturbative treatment for the proton-hydrogen system becomes inapplicable. This regime corresponds to the Balmer-dominated shocks where the behaviour of the electronic wave function is much more complicated than in the low- and high-energy regions. At the intermediate energies ($\sim$25 keV), there is no dominant channel and hence, excitation, electron capture and ionisation are all significant, interconnected and mutually dependent. Therefore, a coupled-channel approach is needed. However, the use of such an approach is difficult as it requires development of two-centre expansions and extensive convergence tests.

The proton-hydrogen collision system has a fundamental significance in scattering theory as it represents a genuine three-body problem where the interactions between all of the particles and the two-body bound state wave functions in reaction channels are analytically known. Hence it allows physicists to test different computational methods on the proton-hydrogen collision system. Achieving an accurate solution for proton scattering on hydrogen is a challenging task as there are infinitely many reaction channels. The latest research on the subject is the development of the quantum-mechanical convergent close-coupling (QM-CCC) [7, 8], semiclassical convergent

close-coupling (SC-CCC) [9] and wave-packet convergent close-coupling (WP-CCC) [10, 11] methods which utilized two different classes of pseudostates for the description of the target atom and the atom formed by the projectile after capturing the electron. The QM-CCC and SC-CCC methods used a basis of Laguerre pseudostates, while WP-CCC used a basis obtained from combining eigenstates and continuum wave packets. Irrespective of their size each of these bases form an orthonormal and square-integrable set which is well suited for expansion of the total scattering wave function. Therefore, all of these three close-coupling approaches allow one to obtain various cross sections convergent with respect to the increasing size of the utilized basis. The Laguerre and the wave-packet bases have their own merits and disadvantages. The basis of the Laguerre pseudostates is more convenient in the practical sense as their radial extent is much shorter and, therefore, pose less difficulties in matrix elements calculations. On the other hand, the basis of wave-packet pseudostates allows one to generate pseudostates with arbitrary energies making it ideal for differential ionization studies. The strength of these methods and also other approaches based on the two-center close-coupling scheme is that they are capable of providing cross sections for elastic scattering, excitation, electron-capture and ionization processes on the state-selective level. This fact allows to calculate various quantities which have great significance in other branches of physics such as astrophysics as discussed above.

There is a consensus between experiment and theory as far as the linear polarization of Lyman-α emission is concerned [9, 12]. The experimental measurements of Balmer-α emission were performed by Donnelly *et al.* [13] and by Detleffsen *et al.* [14]. The experimental data of Donnelly *et al.* [13] gave rise to an estimated uncertainty of $\pm 21\%$ due to the normalisation procedure. The data disagree with the results of close-coupling calculations (see McLaughlin *et al.* [15] and references therein). Additionally, comparison of the experimental measurements of Donnelly *et al.* [13] with the more recent theoretical results of Winter [16], revealed a factor of 2 disagreement for Balmer-α emission. On the other hand, the experimental data obtained by Detleffsen *et al.* [14] showed some agreement with the theoretical calculations, but the experimental uncertainties were quite large which was due to subtracting two cross sections of similar magnitudes. Tseliakhovich *et al.* [4] calculated Balmer emission by solving the Schrödinger equation directly using a lattice technique. The approach produced Balmer-α emission cross sections that are in line with the results of the previous close-coupling calculations and the disagreement with experiment still remains. This warrants further and more thorough studies on the subject. The main goal of the current paper is to use the wave-packet implementation of the convergent close-coupling (CCC) approach to calculate the Balmer emission cross sections.

The paper is set out as follows. In Sect. II we give a brief outline of the two-center WP-CCC method. The results of calculations are presented in Sect. III. Finally, in Sect. IV we highlight the main results and draw conclusions. Unless specified otherwise, atomic units are used throughout this manuscript.

II. TWO-CENTRE WAVE-PACKET CONVERGENT CLOSE-COUPLING METHOD

We consider scattering of a proton on atomic hydrogen. The target nucleus is located at the origin and the projectile is assumed to be moving with a velocity $\boldsymbol{v}$ along a straight-line

$$\boldsymbol{R} = \boldsymbol{b} + \boldsymbol{v}t, \tag{1}$$

where $\boldsymbol{b}$ is the impact parameter and $\boldsymbol{b}\cdot\boldsymbol{v} = 0$. In what follows the index α denotes a full set of principal (n), orbital (l) and magnetic (m) quantum numbers of a state in a channel where projectile of relative momentum $\boldsymbol{q}_\alpha$ is incident on a bound state of the target atom. Index β denotes a quantum state in the rearrangement channel, where the atom formed by the projectile after electron capture has momentum $\boldsymbol{q}_\beta$ relative to the stripped target nucleus. The position of the projectile with respect to the centre of mass of the target nucleus-electron pair is denoted by $\boldsymbol{\rho}$, while $\boldsymbol{\sigma}$ is the position of the projectile-electron pair with respect to the target nucleus. The position of the electron relative to the target proton is $\boldsymbol{r}_\mathrm{T}$, while $\boldsymbol{r}_\mathrm{P}$ is the electron's position relative to the projectile.

We treat the proton-hydrogen collision system within the two-centre convergent-close coupling approach which starts from the exact three-body formalism [11], where the total three-body scattering wave function Ψ_i^+ fulfils the exact Schrödinger equation

$$(H - E)\Psi_i^+ = 0, \tag{2}$$

where E is the total energy and H is the full three-body Hamiltonian of the collision system. Index i denotes the initial channel, from which the total scattering wave develops. In the present work it is taken to be the projectile of energy E_in incident on H in the ground state. The solution of the Schrödinger equation (2) is represented as

$$\Psi_i^+ \approx \sum_{\alpha=1}^{N} F_\alpha(t,\boldsymbol{b}) e^{i\boldsymbol{q}_\alpha\cdot\boldsymbol{\rho}}\psi_\alpha(\boldsymbol{r}_\mathrm{T}) + \sum_{\beta=1}^{M} G_\beta(t,\boldsymbol{b}) e^{i\boldsymbol{q}_\beta\cdot\boldsymbol{\sigma}}\psi_\beta(\boldsymbol{r}_\mathrm{P}), \tag{3}$$

where ψ_α and ψ_β are the target- and projectile-centred pseudostates, and N and M are the numbers of basis functions on the target and projectile centers, respectively. Before the collision ($t = -\infty$) the channel wave function is given as $e^{i\boldsymbol{q}_\alpha\cdot\boldsymbol{\rho}}\psi_i(\boldsymbol{r}_\mathrm{T})$. After the collision ($t \to +\infty$) the expansion coefficients $F_\alpha(+\infty,\boldsymbol{b})$ and $G_\beta(+\infty,\boldsymbol{b})$ represent the transition amplitudes (in the impact-parameter representation) into the target and projectile pseudostates.

By substituting the expansion (3) of the total scattering wave function into Eq. (2) and using a semiclassical approximation, the Schrödinger equation is converted (see Abdurakhmanov *et al.* [11] for details) into the following system of coupled differential equations for the expansion coefficients $F_\alpha(t,\boldsymbol{b})$ and $G_\beta(t,\boldsymbol{b})$:

$$\begin{cases} i\dot{F}_{\alpha'} + i\sum_{\beta=1}^{M}\dot{G}_\beta\tilde{K}_{\alpha'\beta} = \sum_{\alpha=1}^{N}F_\alpha D_{\alpha'\alpha} + \sum_{\beta=1}^{M}G_\beta\tilde{Q}_{\alpha'\beta}, \\ i\sum_{\alpha=1}^{N}\dot{F}_\alpha K_{\beta'\alpha} + i\dot{G}_{\beta'} = \sum_{\alpha=1}^{N}F_\alpha Q_{\beta'\alpha} + \sum_{\beta=1}^{M}G_\beta\tilde{D}_{\beta'\beta}, \\ \alpha' = 1,2,\ldots,N, \quad \beta' = 1,2,\ldots,M, \end{cases} \tag{4}$$

where dots over F_α and G_β denote time derivative. For the sake of brevity the $\boldsymbol{b}$ and t dependences of the expansion coefficients $F_\alpha(\boldsymbol{b},t)$ and $G_\beta(\boldsymbol{b},t)$, and matrix elements $D_{\alpha'\alpha}(\boldsymbol{b},t)$, $\tilde{D}_{\beta'\beta}(\boldsymbol{b},t)$, $K_{\beta'\alpha}(\boldsymbol{b},t)$, $\tilde{K}_{\alpha'\beta}(\boldsymbol{b},t)$, $Q_{\beta'\alpha}(\boldsymbol{b},t)$ and $\tilde{Q}_{\alpha'\beta}(\boldsymbol{b},t)$ are omitted. In this work, for the description of the hydrogen target and the atom formed after the projectile capturing the target electron we employ a basis of wave functions constructed from the combination of the hydrogen bound eigenstates and continuum wavepacket pseudostates. For this case, the details of the derivations and the expressions for the matrix elements are given in [11]. Due the cylindrical symmetry of the collision the dependence of the expansion coefficients and matrix elements on the azimuthal angle of vector $\boldsymbol{b}$ can be factored out as a phase factor and then canceled. As a result the set of equations (4) is transformed to the form where there is no dependence on the angular part of $\boldsymbol{b}$. This transformed set of equations is solved subject to the initial-state boundary condition specified as

$$\begin{cases} F_{\alpha i}(-\infty,b) = \delta_{\alpha i}, & \alpha = 1,2,\ldots,N, \\ G_{\beta i}(-\infty,b) = 0, & \beta = 1,2,\ldots,M. \end{cases} \tag{5}$$

Calculations of the Balmer-α emission cross section and polarization fraction require evaluations of the partial cross sections for the direct-scattering processes leading to excitation of the target. The partial cross sections for the individual direct-scattering (denoted as di) and electron-capture (denoted as ec) transitions from the ground state of hydrogen are given as

$$\sigma_\alpha^{\rm di} = 2\pi\int_0^\infty db\; bP_\alpha^{\rm di}(b), \tag{6}$$

$$\sigma_\beta^{\rm ec} = 2\pi\int_0^\infty db\; bP_\beta^{\rm ec}(b), \tag{7}$$

respectively, where the transition probabilities are

$$P_\alpha^{\rm di}(b) = |F_{\alpha i}(+\infty,b) - \delta_{\alpha i}|^2, \tag{8}$$

$$P_\beta^{\rm ec}(b) = |G_{\beta i}(+\infty,b)|^2. \tag{9}$$

III. RESULTS AND DISCUSSION

As mentioned in the previous section the calculation of the Balmer-α emission cross section requires accurate computations of the cross sections for electron excitation into the $3s, 3p_0, 3p_{\pm1}, 3d_{\pm1}$ and $3d_{\pm2}$ states. To this end we performed calculations using the WP-CCC method with the set of numerical parameters which produced fully convergent results for the state-resolved excitation and electron-capture cross sections for the transitions to the final states with principal quantum number $n \leq 4$ [18]. To be more specific we adopted a symmetric two-center treatment of the proton-hydrogen scattering problem and employed two identical bases for the description of the target and projectile centers. In this model accurate final results can be obtained by examining their convergence with respect to the parameters characterizing the motion of the projectile and the structure of the target and the projectile-electron system, such as the maximum included orbital angular momentum quantum number $l_{\rm max}$, the number of bound (negative-energy) eigenstates $N_{\rm b} - l$, the maximum energy $\varepsilon_{\rm max}(= \kappa_{\rm max}^2/2)$ of the electron continuum covered by the wavepacket bins, and the number of bins within this interval $N_{\rm c}$. Each of these parameters is systematically increased while fixing the others at sufficiently large values. The largest calculations, which yielded converged cross sections for all considered transitions, employed a total of 2534 states (1267 on each center), where for each angular momentum $l \leq 6$ $10 - l$ bound states and $N_{\rm c} = 20$ continuum wavepacket pseudostates. The system of scattering equations (4) was solved using the standard Runge-Kutta method by varying the z-component of the projectile position from -100 to $+100$ a.u. at all incident energies. Setting the upper limit for the impact parameter $b_{\rm max}$ required additional attention as the probabilities for some considered transitions decayed significantly slower than others when this parameter is increased. It was established that $b_{\rm max} = 50$ a.u. was adequate for the cross section calculations in the low and the intermediate energy region, while it was not large enough for the greater energies. This is mainly because of the probabilities for the $2p_0$, $2p_1$, $3p_0$ and $3p_1$ transitions having extremely long tails. As the energy increases, the tail becomes longer and, therefore, to achieve convergent and smooth cross sections, larger impact parameters should be used. As a result of this, $b_{\rm max}$ was increased to 70 a.u. within the energy region of $500-1000$ keV.

Before conducting calculations for Balmer-α emission we verified that the calculations with the aforementioned numerical parameters produce reliable results for the linear polarization of Lyman-α emission. The current WP-CCC calculations produced the Lyman-α emission cross sections that are in excellent agreement with the results of our previous calculations that used a different two-center basis constructed from Laguerre pseudostates.

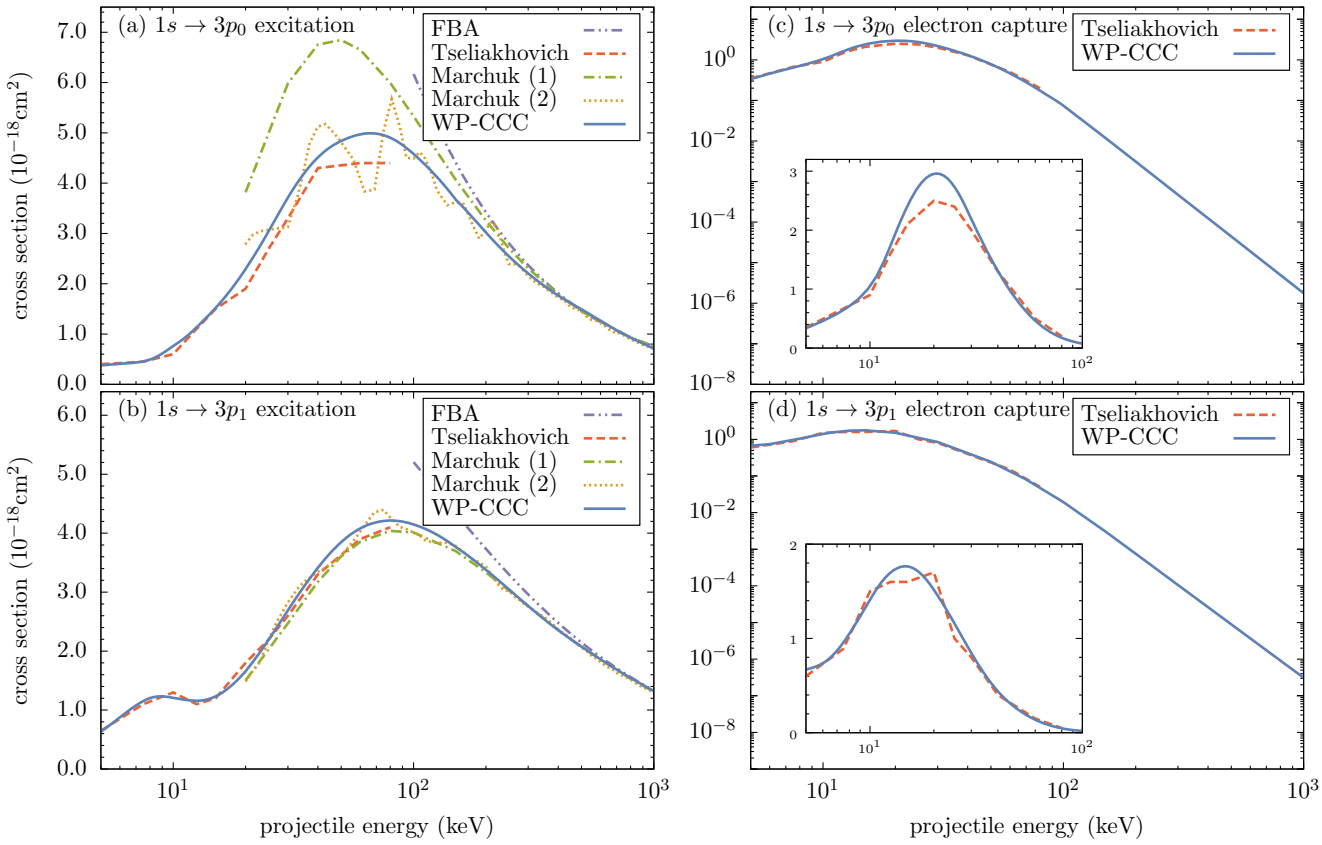

FIG. 1. The m-resolved cross sections for excitation and electron capture into the $3p$ subshell in p-H($1s$) collisions. The present WP-CCC results are compared with the calculations of Tseliakhovich *et al.* [4] based on the direct solution of Schrödinger equation, the AOCC (1) and the Glauber approximation (2) calculations of Marchuk *et al.* [17], as well as the FBA results. The inserts in electron-capture panels show the same using a linear scale on the ordinate axis.

A. Excitation and electron capture into the $n = 3$ and $n = 4$ shell states

In order to investigate Balmer emission, a full set of calculations were carried out for the cross sections of electron excitation into the all lm-resolved $n = 3$ and $n = 4$ shell states. These partial cross sections were then used to calculate the excitation cross sections for the $3p$, $3d$, $4p$, $4d$ and $4f$ states as well as the $n = 3$ and $n = 4$ shell as a whole.

Figures 1 and 2 show the m-resolved cross sections for excitation and electron capture into the $3p$ and $3d$ subshells, respectively. These magnetic sublevel populations of the excited states provide a stringent test of the theory. We see substantial variations between the results of various theoretical approaches. The results of Tseliakhovich *et al.* [4], computed by solving the Schrödinger equation using a lattice method, seem to be in better agreement with ours, however even here we see significant deviations. In particular, there is up to 20% disagreement in the cross sections for electron capture into the $3p_0$ state (see panel c in Fig. 1) and up to 30% disagreement in the cross sections for excitation of the $3d$ shell states (panels a, b and c in Fig. 2), when the WP-CCC results are compared with those of Tseliakhovich *et al.* [4]. Disagreement between the present excitation cross sections and those of Marchuk *et al.* [17] are significantly larger for all levels except for excitation of the $3p_1$ one. The results presented above will later be used to calculate the polarization fraction of the proton-impact induced Balmer-α radiation of hydrogen.

The excitation and electron capture cross sections summed over m are shown in Fig. 3. As one can see our $3s$ excitation cross section (see panel a) displays overall good agreement with Winter's 220-state Sturmian function calculations [16] and the results of Tseliakhovich *et al.* [4]. The present $3p$ excitation cross section (panel b) displays excellent agreement with the experimental measurements of Detleffsen *et al.* [14]. In addition, below 40 keV our $3p$ excitation cross section agrees well with the theoretical results of Winter [16] and Tseliakhovich *et al.* [4]. In contrast to the $3s$ and $3p$ excitation cross sections, the agreement between our $3d$ excitation cross section (panel c) and the other theoretical data is not very good. The cross sections for electron capture into $3s, 3p$ and $3d$ states are shown in panels d, e and f, respectively, in comparison with the existing theoretical data. Agreement between our results and the theoreti-

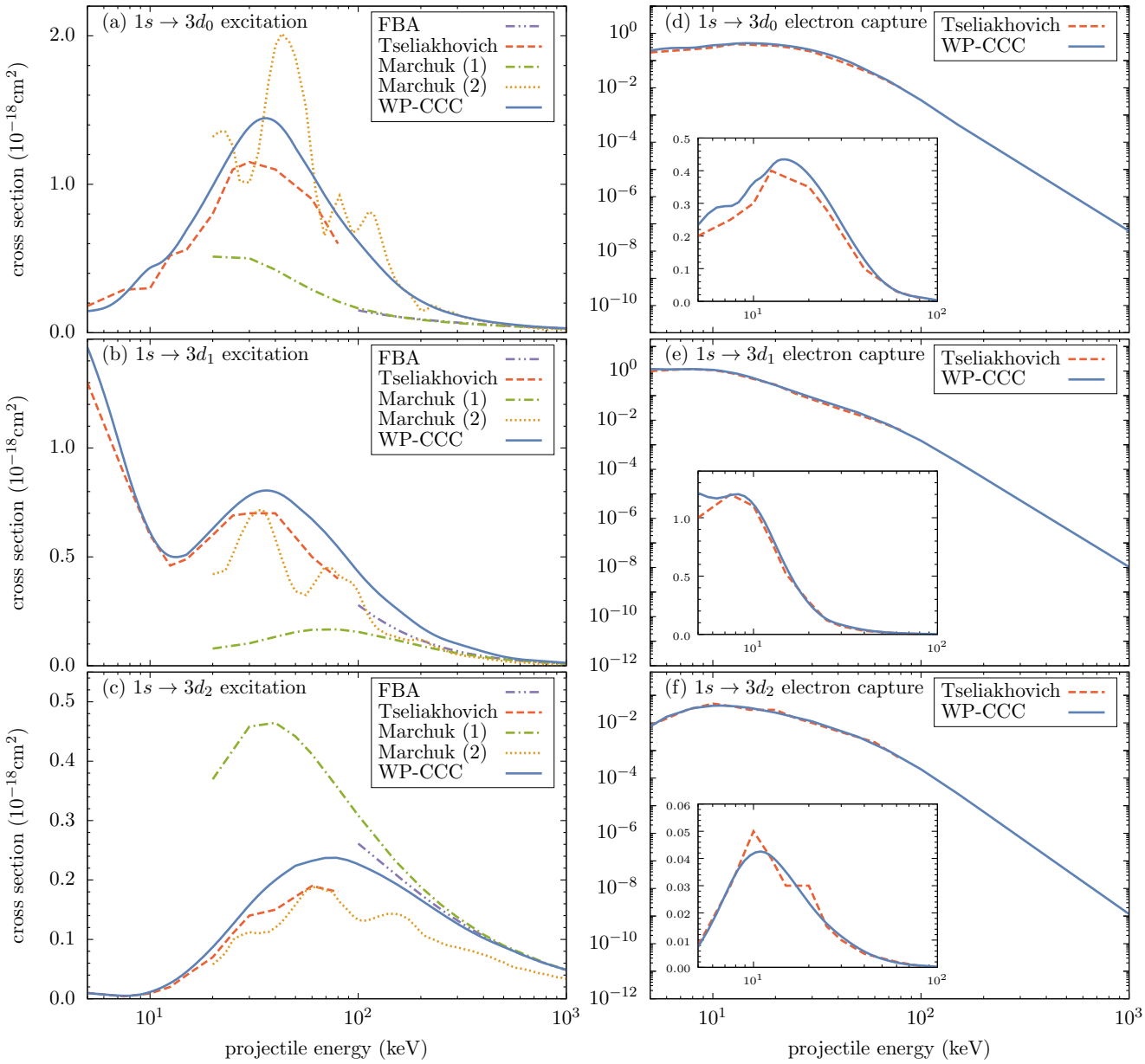

FIG. 2. The m-resolved cross sections for excitation and electron capture into the $3d$ subshell in p-H($1s$) collisions. The present WP-CCC results are compared with the calculations of Tseliakhovich *et al.* [4] based on the direct solution of Schrödinger equation, the AOCC (1) and the Glauber approximation (2) calculations of Marchuk *et al.* [17], as well as the FBA results. The inserts in electron-capture panels show the same using a linear scale on the ordinate axis.

cal calculations of Winter [16] and Tseliakhovich *et al.* [4] is generally quite good, though some disagreement is noticeable in the linear scale as shown in the inserts.

In Fig. 4 we present the excitation cross section into the $n = 3$ shell in comparison with the experimental results of Park *et al.* [20]. The experimental data lie higher than our results within the energy region of $50 - 100$ keV where the cross section peaks. However, this disagreement appears to be systematic as it is observed for the other theoretical results as well, with the latter agreeing with each other reasonable well.

Overall, our excitation and electron capture cross section calculations into $3s, 3p$ and $3d$ states show reasonable agreement with the available theoretical data provided by Winter [16] and Tseliakhovich *et al.* [4] with the WP-CCC calculations spanning a much wider energy range. Agreement between our values and the experimental measurements of Detleffsen *et al.* [14] for excitation into $3p$ state is excellent, whereas there is clear disagreement between our results and the experimental data of Park *et al.* [20] for the cross section of excitation of the $n = 3$ state. Our calculations show that around the maximum the contributions of the 3s and 3d cross sections to the $n = 3$ cross section are considerably smaller than

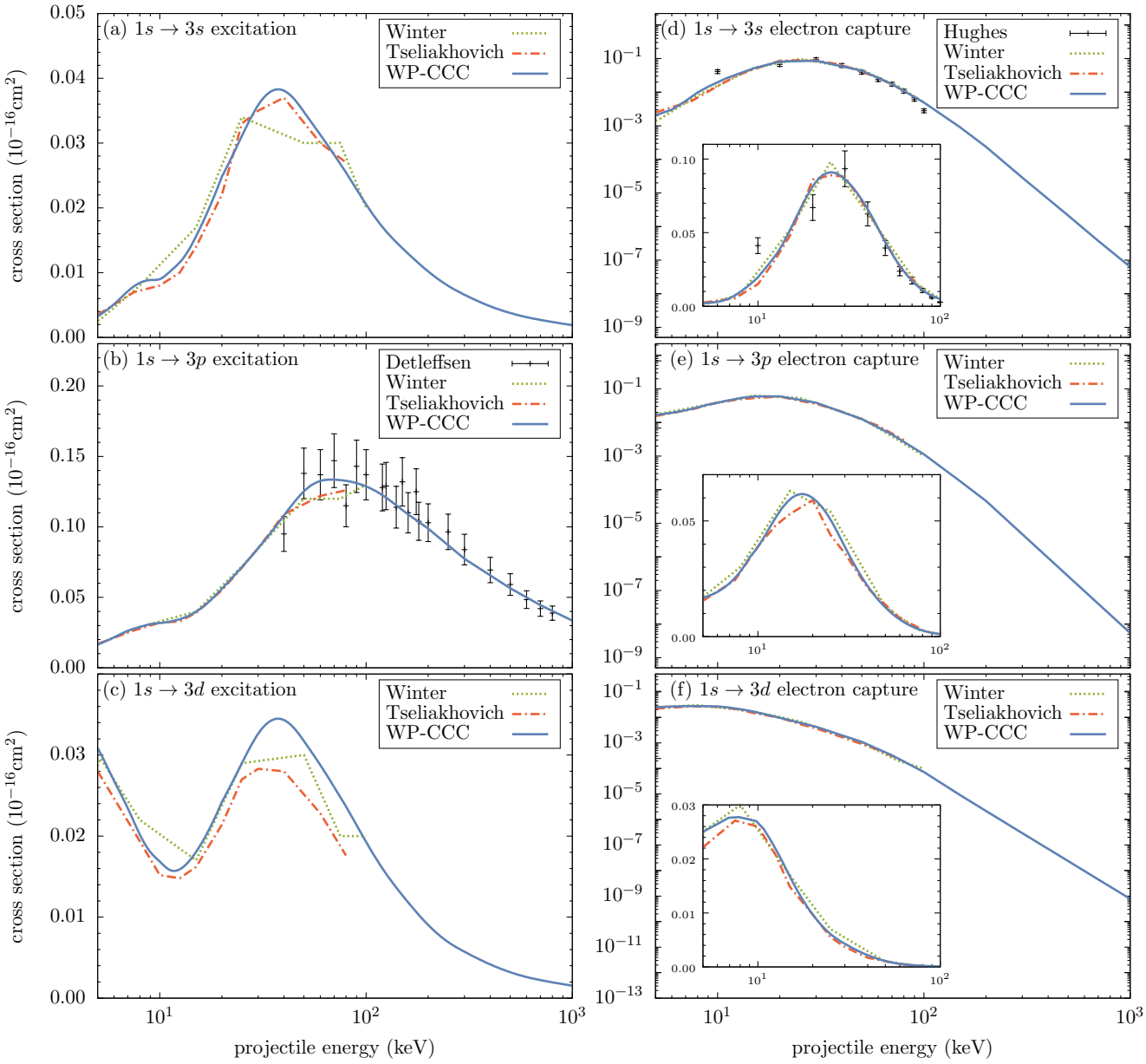

FIG. 3. The cross sections for excitation and electron capture into the $n = 3$ shell states in p-H($1s$) collisions. The present WP-CCC results are compared with the theoretical calculations of Winter [16] and Tseliakhovich *et al.* [4]. The experimental data for $3p$ excitation and $3s$ electron capture are due to Detleffsen *et al.* [14] and Hughes *et al.* [19], respectively.

the dominant 3p cross section.

A similar picture is observed for the cross sections for excitation and electron capture into the $n = 4$ shell states as shown in Figs. 5-6. Here also the present $4p$ excitation cross section (Fig. 5, panel b) displays excellent agreement with the experimental measurements of Detleffsen *et al.* [14], while the total $n = 4$ cross section is again smaller than the experimental data of Park *et al.* [20] (Fig. 6, panel a). There is reasonable agreement between present results and calculations of Tseliakhovich *et al.* [4] for all considered $n = 4$ shell cross sections both for excitation and electron capture. There is also good agreement with the results of Belkic *et al.* [21] for electron capture at higher energies.

B. Balmer emission

Here we investigate the behaviour of parameters characterising Balmer emission with changing impact energy of incident protons. The Balmer-α emission cross section can be expressed in terms of the excitation cross sections to the different l-states of the $n = 3$ shell as [13]

$$\sigma(\mathrm{H}\alpha) = \sigma^{\mathrm{di}}_{3s} + B_{3p,2s}\sigma^{\mathrm{di}}_{3p} + \sigma^{\mathrm{di}}_{3d}. \qquad (10)$$

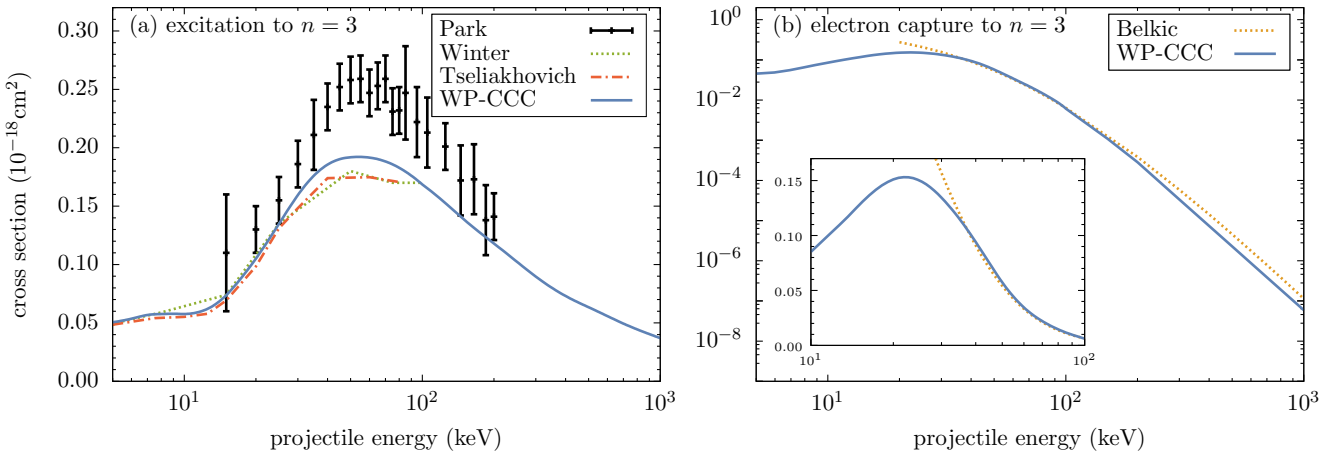

FIG. 4. The cross section for excitation and electron capture into the $n = 3$ shell states in p-H($1s$) collisions. The present WP-CCC results for excitation are compared with experimental data of Park *et al.* [20] and theoretical calculations by Winter [16] and Tseliakhovich *et al.* [4]. The present results for electron capture are compared with the first-order boundary-corrected calculations of Belkic *et al.* [21].

The polarization fraction of the proton impact induced Balmer-α radiation of hydrogen is written as [22]

$$\Pi(\mathrm{H}\alpha) = \left[B_{3p,2s} \frac{\sigma^{\mathrm{di}}_{3p_0} - \sigma^{\mathrm{di}}_{3p_1}}{2} + 57 \frac{\sigma^{\mathrm{di}}_{3d_0} + \sigma^{\mathrm{di}}_{3d_1} - \sigma^{\mathrm{di}}_{3d_2}}{100} \right] \times \left[\sigma^{\mathrm{di}}_{3s} + B_{3p,2s} \frac{7\sigma^{\mathrm{di}}_{3p_0} + 11\sigma^{\mathrm{di}}_{3p_1}}{6} + \frac{119\sigma^{\mathrm{di}}_{3d_0} + 219\sigma^{\mathrm{di}}_{3d_1} + 162\sigma^{\mathrm{di}}_{3d_2}}{100} \right]^{-1}. \quad (11)$$

The Balmer decrement of the proton impact induced Balmer radiation of hydrogen is written as [4]

$$\mathrm{H}_\alpha/\mathrm{H}_\beta = \frac{\sigma^{\mathrm{di}}_{3s} + B_{3p,2s}\sigma^{\mathrm{di}}_{3p} + \sigma^{\mathrm{di}}_{3d}}{B_{4s,2p}\sigma^{\mathrm{di}}_{4s} + B_{4p,2s}\sigma^{\mathrm{di}}_{4p} + B_{4d,2p}\sigma^{\mathrm{di}}_{4d}}. \quad (12)$$

The branching ratio coefficients entering Eqs (10-12) are simply the Einstein A-coefficient for a given transition normalised by the Einstein A-coefficients of all of the transitions allowed by the electric dipole selection rule. According to [4]

$$\begin{aligned} B_{3p,2s} &\approx 0.1183, \\ B_{4s,2p} &\approx 0.5841, \\ B_{4p,2s} &\approx 0.1191, \\ B_{4s,2p} &\approx 0.7456. \end{aligned} \quad (13)$$

In Fig. 7, the calculated Balmer-α emission cross section in proton-hydrogen collisions is presented as a function of impact energy. The results of the different theoretical approaches are shown with lines, while the symbols with error bars represent the experimental data. The present results and the calculations of Winter [16] underestimate the experimental values of Donnelly *et al.* [13] by nearly 100% at the energy where the cross section has a maximum. The experimental data of Donnelly *et al.* [13] do not include a contribution from cascades, which is estimated to be up to 15%. This means that the level of disagreement is even worsens if the cascades are included. The errorbars on the data of Donnelly *et al.* [13] show only random errors, while additional ± 21% uncertainties due to normalisation are not shown. A better agreement of the theoretical calculations is observed with the data provided by Detleffsen *et al.* [14], who measured the $\sigma(3p)$ cross section and obtained the Balmer-α emission cross section from the formula $\sigma(\mathrm{H}\alpha) = \sigma(n = 3) - (1 - B_{3p,2s})\sigma(3p)$, where the experimental data for $\sigma(n = 3)$ were measured by Park *et al.* [20]. However, we should note that the data of Park *et al.* [20] for $\sigma(n = 3)$ were normalized to the first Born calculations at 200 keV. Generally, the first Born approximation produces larger cross sections at intermediate energies and becomes more accurate at higher projectile energies. Typical errors in the measurements of Detleffsen *et al.* [14] are shown only for 3 data points. The data include the cascades estimated to be 5%.

The theoretical results discussed above do not include a contribution from cascades. The theoretical calculations of McLaughlin *et al.* [15] without and with cascades (denoted in Fig. 7 as McLaughlin (1) and McLaughlin (2), respectively), lie somewhat higher than the calculations performed by Winter [16] and the present WP-CCC results. Firstly, the cascade contribution estimated by McLaughlin *et al.* [15] appears to be smaller than 15%. Secondly, the calculations of McLaughlin *et al.* [15] reach a maximum value of Balmer-α cross section around $E = 40$ keV, in agreement with a similar behaviour observed in the other theoretical data. However, they show another peak around $E = 145$ keV, most likely due to the limited size of the basis. In contrast to the results of McLaughlin *et al.* [15], the WP-CCC results fall smoothly

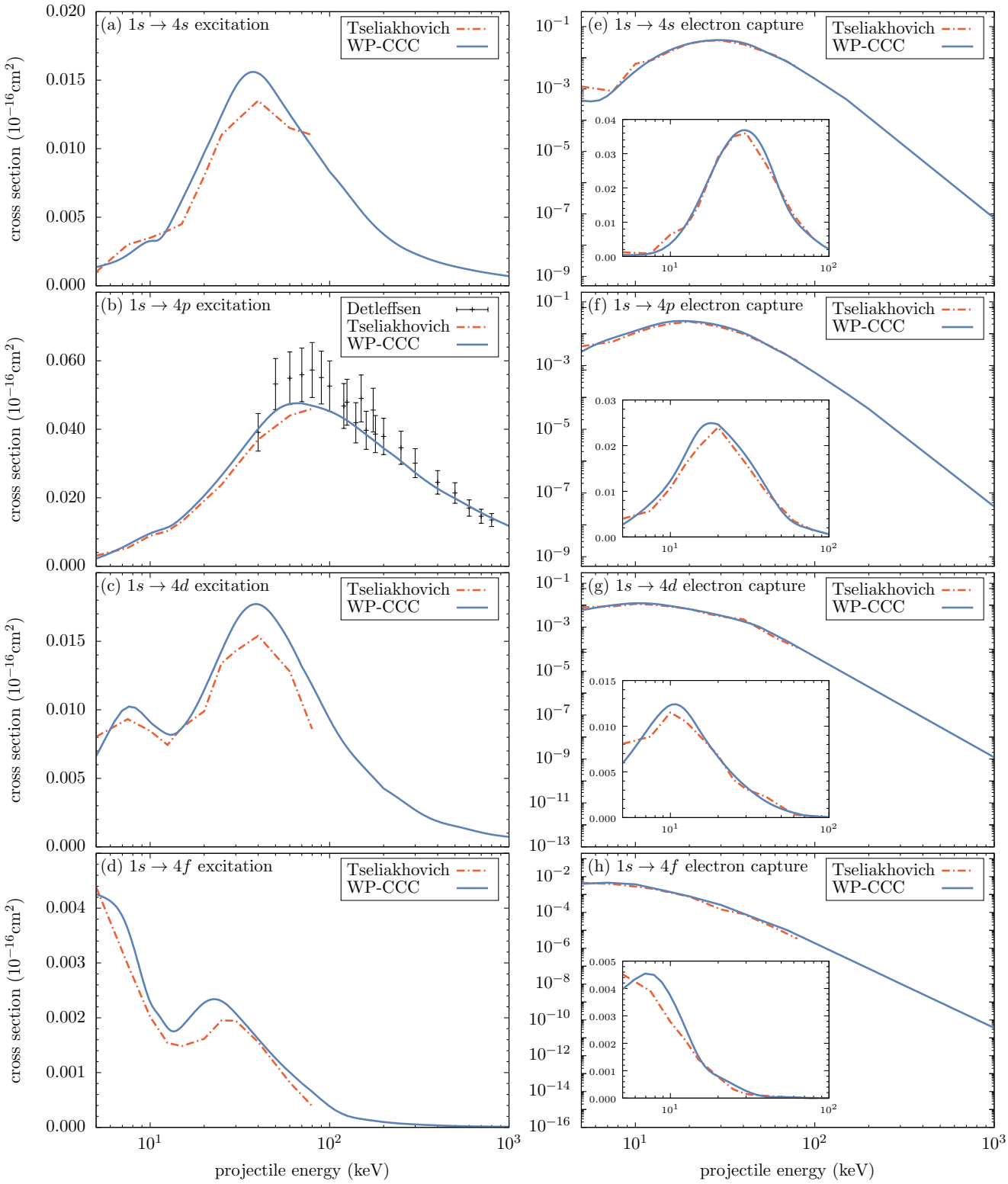

FIG. 5. The cross sections for excitation and electron capture into the $n = 4$ shell states in p-H($1s$) collisions. The present WP-CCC results are compared with the theoretical calculations of Winter [16] and Tseliakhovich *et al.* [4]. The experimental data for $4p$ excitation are due to Detleffsen *et al.* [14].

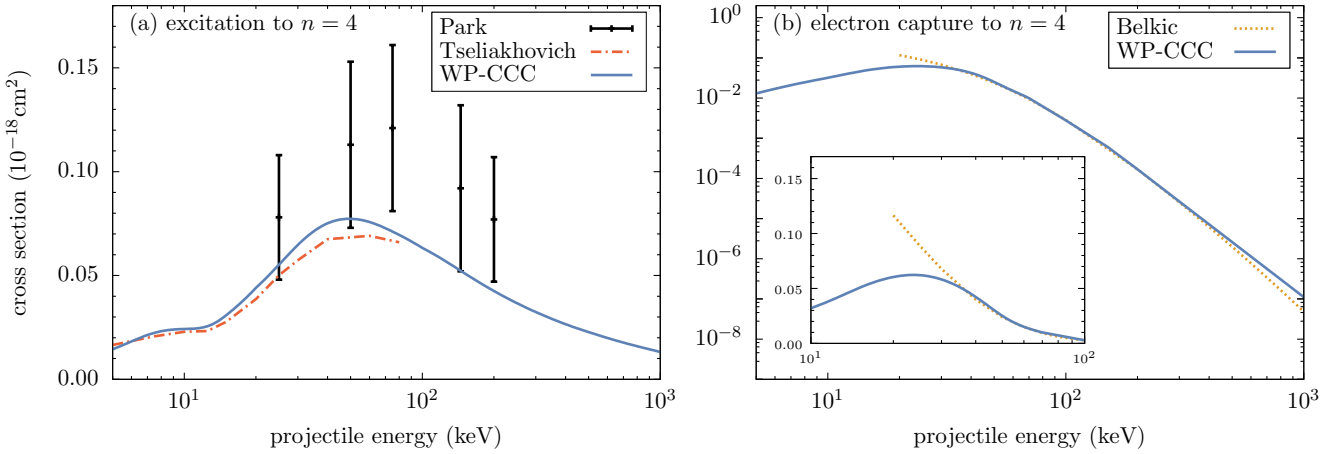

FIG. 6. The cross section for excitation and electron capture into the $n = 4$ shell states in p-H($1s$) collisions. The present WP-CCC results for excitation are compared with experimental data of Park *et al.* [20] and theoretical calculations by Tseliakhovich *et al.* [4]. The present results for electron capture are compared with the first-order boundary-corrected calculations of Belkic *et al.* [21].

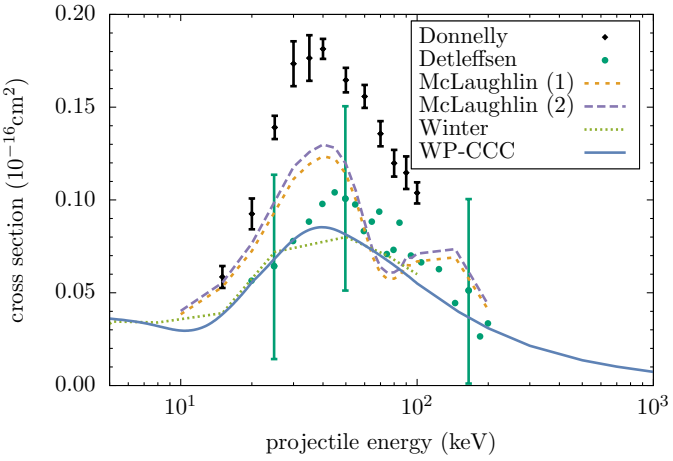

FIG. 7. Balmer-α emission cross section in p-H($1s$) collisions as a function of the impact energy. The present WP-CCC results are compared with the experimental results of Donnelly *et al.* [13] and Detleffsen *et al.* [14] and theoretical calculations of McLaughlin *et al.* [15] [without (1) and with (2) cascades] and Winter [16].

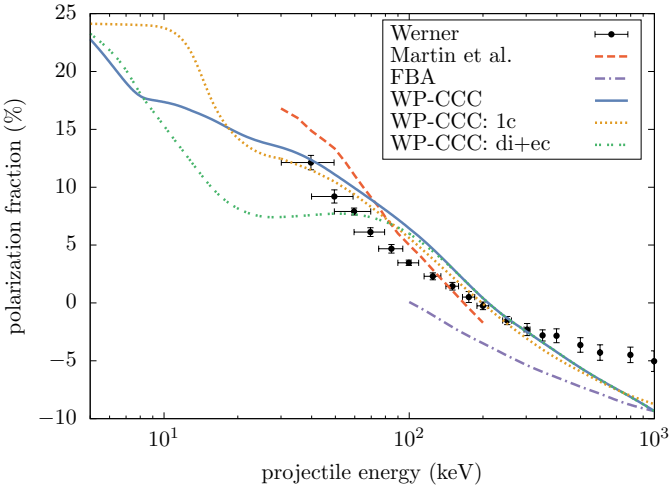

FIG. 8. Polarization fraction of the proton impact induced Balmer-α radiation of hydrogen. The present WP-CCC results are compared with the experimental results of Werner and Schartner [23] and theoretical calculations of Martin [24].

after reaching the maximum value. Moreover, the present calculations display very good agreement with Winter [16] in the energy region of $10 - 100$ keV, but the latter do not go beyond 100 keV.

Thus, even though our results for the Balmer-α emission cross section are significantly lower than the experimental measurements of Donnelly *et al.* [13] and the theoretical calculations of McLaughlin *et al.* [15], they show good agreement with the theoretical data of Winter [16]. They also fall within the error bars of experimental measurements of Detleffsen *et al.* [14] due to the large experimental uncertainty.

In Fig. 8 we present the WP-CCC results (solid line) in comparison with the experimental results of Werner and Schartner [23] and theoretical calculations of Martin [24]. We see reasonably good agreement with the experiment data up to 350 keV. However, at higher energies our results significantly underestimate them. We also present the one-centre WP-CCC results (denoted as WP-CCC: 1c). At high energies the full and one-centre results coincide as the electron transfer channels are negligible and do not influence excitation of the target. This gives us confidence in the accuracy of the present calculations and may indicate that the experimental data above 400 keV is unreliable. We emphasise that the polarization fraction the Balmer-α radiation is calculated using Eq. (11), where the underlying cross sections are for direct excitation of the target hydrogen. For comparison, we also

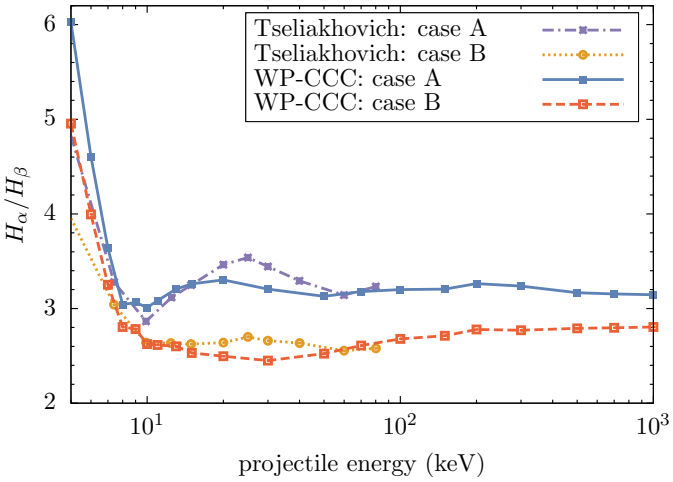

FIG. 9. The Balmer decrement H_α/H_β as a function of the impact energy for hydrogen atom emission induced by protons. The present WP-CCC results are compared with theoretical calculations by Tseliakhovich *et al.* [4].

show the polarization fraction that includes the Balmer-α radiation emitted by the moving hydrogen atom formed by the projectile after capturing the electron (denoted as WP-CCC: di+ec). The latter start deviating from the WP-CCC results below 100 keV as electron capture starts dominating direct excitation.

In the situation when the neutral hydrogen density is small enough for Lyman lines to freely escape the cloud (case A) the branching ratio coefficients are defined as in Eq. (13). When the neutral hydrogen density is large enough for Lyman lines to be trapped (case B) these coefficients are essentially unity.

In Fig. 9 we present the WP-CCC Balmer decrements H_α/H_β for the cases A and B in comparison with theoretical calculations of Tseliakhovich *et al.* [4]. The results suggest that the Balmer decrement plateaus around 100 keV in both cases.

C. The density matrix $\rho^i_{\alpha'\alpha}$

Finally we present the density matrix that is required for plasma modelling and diagnostics. This matrix can be calculated using the probability amplitudes $F_{\alpha i}(+\infty, b)$ as follows:

$$\rho^i_{\alpha'\alpha} = 2\pi \int_0^\infty dbbF^*_{\alpha' i}(+\infty, b)F_{\alpha i}(+\infty, b). \qquad (14)$$

We note that the diagonal matrix elements, $\rho^i_{\alpha\alpha}$, are real and coincide with the integrated cross sections for the individual transition from the initial target state i to the final target state α, i.e $\rho^i_{\alpha\alpha} \equiv \sigma^{\rm di}_\alpha$.

Table I lists the density matrix elements for 50 keV proton scattering on the ground state of hydrogen. Similar data but obtained using the atomic orbital close coupling method were given by Schultz and Ovchinnikov [25] at 50 and 60 keV. The density matrices for excited initial states of hydrogen were given in [18]. One can notice that the diagonal matrix elements are real. These represent the corresponding excitation cross sections. In this work we give sample results for the density matrices at one incident energy. The full set of results will be available through the IAEA Atomic and Molecular Data Unit in due time. In addition, results at any other projectile energies in the interval from 5 keV and 1 MeV can be requested from the authors.

IV. CONCLUSIONS

The wavepacket based semiclassical two-centre convergent close-coupling method for the proton scattering from the hydrogen atom has been implemented to calculate the Balmer emission cross section and polarization fraction which play an important role in astrophysical shocks. The three-body Schrödinger equation has been solved by expanding the total scattering wave function in a two-center orthonormal basis set constructed from the hydrogen eigenstates and continuum wavepackets. The cross sections necessary for the Balmer emission cross section and polarization fraction have been calculated. Substantial variations between the results of various theoretical approaches have been found for the magnetic sublevel populations of the excited states that provide a stringent test of the theory. The obtained Balmer-α emission cross section is found to be significantly lower than the experimental measurements of Donnelly *et al.* [13]. However, there is reasonably good agreement with the data of Detleffsen *et al.* [14]. Our results differ from the theoretical calculations of McLaughlin *et al.* [15] with and without cascading, however, they support the results of Winter [16] and Tseliakhovich *et al.* [4]. Present results for the polarization fraction of the Balmer-α radiation of hydrogen do not agree with the experimental data by Werner and Schartner [23] above 400 keV. Convergence studies have been performed to support the accuracy of the present calculations. Accordingly we question the accuracy of the experimental polarization fraction at high energies.

ACKNOWLEDGEMENTS

This work was supported by the Australian Research Council, the Pawsey Supercomputer Centre, and the National Computing Infrastructure. A.S.K. acknowledges a partial support from the U.S. National Science Foundation under Award No. PHY-1415656. A.M.M. acknowledges support from the U.S. DOE Grant No. DE-FG02-93ER40773, the U.S. NSF Grant No. PHY-1415656, and the NNSA Grant No. DE-NA0003841.

TABLE I. Density matrix elements $\rho^{1s}_{\alpha'\alpha}$ (in 10^{-16}cm^2) for excitation of H($1s$) into the final n =1-4 shell states of the target by proton impact at 50 keV. Notation: A[-N] implies A$\times 10^{-\mathrm{N}}$, the final states α' and α are given in nlm notations.

α'	α	Re	Im	α'	α	Re	Im	α'	α	Re	Im	α'	α	Re	Im
100	100	6.18[-1]	0	210	321	-2.25[-2]	-4.16[-2]	310	420	-1.74[-2]	4.21[-3]	400	431	-1.31[-3]	9.25[-4]
100	200	-1.41[-1]	-1.79[-1]	210	322	1.22[-2]	-2.19[-2]	310	421	-8.70[-3]	-1.01[-2]	400	432	-6.09[-4]	-2.39[-4]
100	210	1.74[-1]	5.69[-2]	210	410	6.98[-2]	2.25[-2]	310	422	2.02[-3]	-6.29[-3]	400	433	-5.24[-5]	-2.21[-4]
100	211	-1.57[-2]	1.42[-1]	210	411	1.46[-3]	6.26[-2]	310	430	3.71[-3]	-3.07[-3]	410	410	1.84[-2]	0
100	300	-5.18[-2]	-9.42[-2]	210	420	-4.37[-2]	1.18[-3]	310	431	3.51[-3]	1.39[-3]	410	411	5.51[-3]	1.43[-2]
100	310	7.24[-2]	4.74[-2]	210	421	-1.63[-2]	-2.94[-2]	310	432	3.52[-4]	1.84[-3]	410	420	-1.06[-2]	3.66[-3]
100	311	-8.04[-3]	6.44[-2]	210	422	8.39[-3]	-1.48[-2]	310	433	-5.11[-4]	5.28[-4]	410	421	-5.95[-3]	-5.57[-3]
100	320	-4.79[-2]	-9.72[-3]	210	430	1.03[-2]	-5.37[-3]	311	311	3.85[-2]	0	410	422	7.78[-4]	-3.88[-3]
100	321	-2.98[-3]	-2.75[-2]	210	431	7.96[-3]	5.14[-3]	311	321	-1.49[-2]	7.21[-3]	410	430	2.15[-3]	-2.15[-3]
100	322	9.72[-3]	-6.20[-3]	210	432	-1.72[-6]	4.85[-3]	311	322	-7.62[-3]	-4.19[-3]	410	431	2.22[-3]	6.29[-4]
100	400	-2.95[-2]	-6.06[-2]	210	433	-1.59[-3]	1.12[-3]	311	411	2.28[-2]	6.88[-4]	410	432	3.20[-4]	1.07[-3]
100	410	4.48[-2]	3.47[-2]	211	211	2.29[-1]	0	311	421	-1.06[-2]	5.20[-3]	410	433	-2.68[-4]	3.38[-4]
100	411	-4.91[-3]	3.92[-2]	211	311	9.23[-2]	9.45[-3]	311	422	-5.18[-3]	-2.93[-3]	411	411	1.35[-2]	0
100	420	-3.74[-2]	-8.92[-3]	211	321	-3.81[-2]	1.45[-2]	311	431	1.96[-3]	-2.66[-3]	411	421	-6.19[-3]	3.23[-3]
100	421	-2.89[-3]	-2.00[-2]	211	322	-1.80[-2]	-1.27[-2]	311	432	1.65[-3]	9.64[-6]	411	422	-3.09[-3]	-1.61[-3]
100	422	6.72[-3]	-4.44[-3]	211	411	5.42[-2]	7.21[-3]	311	433	3.89[-4]	5.14[-4]	411	431	1.12[-3]	-1.59[-3]
100	430	1.06[-2]	-2.99[-3]	211	421	-2.70[-2]	1.04[-2]	320	320	1.25[-2]	0	411	432	9.60[-4]	-2.21[-5]
100	431	3.15[-3]	4.91[-3]	211	422	-1.21[-2]	-8.75[-3]	320	321	3.44[-3]	8.54[-3]	411	433	2.34[-4]	2.88[-4]
100	432	-1.30[-3]	1.84[-3]	211	431	5.27[-3]	-6.12[-3]	320	322	-2.76[-3]	3.67[-3]	420	420	7.06[-3]	0
100	433	-7.44[-4]	-7.69[-5]	211	432	4.18[-3]	4.28[-4]	320	420	9.32[-3]	6.03[-4]	420	421	2.26[-3]	4.28[-3]
200	200	1.59[-1]	0	211	433	8.70[-4]	1.46[-3]	320	421	2.57[-3]	6.05[-3]	420	422	-1.16[-3]	1.91[-3]
200	210	-1.02[-1]	1.45[-1]	300	300	3.48[-2]	0	320	422	-1.88[-3]	2.50[-3]	420	430	-1.77[-3]	8.73[-4]
200	211	-1.35[-1]	-5.81[-2]	300	310	-2.08[-2]	2.66[-2]	320	430	-2.37[-3]	1.00[-3]	420	431	-1.13[-3]	-8.00[-4]
200	300	7.30[-2]	1.43[-2]	300	311	-2.84[-2]	-7.47[-3]	320	431	-1.45[-3]	-1.20[-3]	420	432	5.33[-5]	-6.37[-4]
200	310	-5.66[-2]	4.82[-2]	300	320	7.08[-3]	-1.70[-2]	320	432	1.45[-4]	-8.88[-4]	420	433	2.11[-4]	-1.13[-4]
200	311	-5.75[-2]	-2.92[-2]	300	321	1.21[-2]	-1.02[-3]	320	433	3.17[-4]	-1.41[-4]	421	421	3.74[-3]	0
200	320	2.25[-2]	-3.35[-2]	300	322	3.36[-3]	4.17[-3]	321	321	7.39[-3]	0	421	422	1.01[-3]	1.60[-3]
200	321	2.66[-2]	3.30[-3]	300	400	2.21[-2]	1.07[-3]	321	322	2.13[-3]	3.30[-3]	421	431	-9.30[-4]	4.92[-4]
200	322	5.39[-3]	1.07[-2]	300	410	-1.51[-2]	1.55[-2]	321	421	5.25[-3]	-4.87[-5]	421	432	-4.69[-4]	-2.55[-4]
200	400	4.59[-2]	1.14[-2]	300	411	-1.70[-2]	-4.80[-3]	321	422	1.43[-3]	2.26[-3]	421	433	-2.69[-5]	-2.10[-4]
200	410	-3.92[-2]	2.68[-2]	300	420	6.41[-3]	-1.29[-2]	321	431	-1.30[-3]	7.09[-4]	422	422	1.03[-3]	0
200	411	-3.43[-2]	-1.82[-2]	300	421	8.76[-3]	-9.05[-4]	321	432	-6.70[-4]	-3.59[-4]	422	432	-2.48[-4]	1.50[-4]
200	420	1.92[-2]	-2.48[-2]	300	422	2.34[-3]	2.89[-3]	321	433	-3.94[-5]	-3.01[-4]	422	433	-1.13[-4]	-4.40[-5]
200	421	1.94[-2]	2.03[-3]	300	430	-4.90[-5]	4.16[-3]	322	322	2.24[-3]	0	430	430	5.64[-4]	0
200	422	3.76[-3]	7.42[-3]	300	431	-2.13[-3]	1.31[-3]	322	422	1.52[-3]	2.59[-5]	430	431	1.78[-4]	3.26[-4]
200	430	-1.86[-3]	8.84[-3]	300	432	-9.17[-4]	-4.51[-4]	322	432	-3.71[-4]	2.18[-4]	430	432	-8.67[-5]	1.37[-4]
200	431	-5.21[-3]	1.87[-3]	300	433	-4.89[-5]	-3.53[-4]	322	433	-1.67[-4]	-6.93[-5]	430	433	-5.84[-5]	-1.90[-6]
200	432	-1.81[-3]	-1.42[-3]	310	310	4.84[-2]	0	400	400	1.41[-2]	0	431	431	2.99[-4]	0
200	433	5.89[-5]	-8.05[-4]	310	311	1.13[-2]	4.06[-2]	400	410	-8.97[-3]	1.05[-2]	431	432	7.99[-5]	1.27[-4]
210	210	3.06[-1]	0	310	320	-2.30[-2]	7.45[-3]	400	411	-1.11[-2]	-2.40[-3]	431	433	-2.33[-5]	5.43[-5]
210	211	3.50[-2]	2.60[-1]	310	321	-1.20[-2]	-1.43[-2]	400	420	3.61[-3]	-8.41[-3]	432	432	8.37[-5]	0
210	310	1.18[-1]	2.48[-2]	310	322	2.91[-3]	-9.23[-3]	400	421	5.57[-3]	-9.57[-4]	432	433	2.06[-5]	2.87[-5]
210	311	5.15[-3]	1.06[-1]	310	410	2.95[-2]	3.03[-3]	400	422	1.65[-3]	1.73[-3]	433	433	1.57[-5]	0
210	320	-5.92[-2]	6.46[-3]	310	411	6.16[-3]	2.41[-2]	400	430	1.07[-4]	2.64[-3]				

[1] K. Heng, Publ. Astron. Soc. Aust. **27**, 23 (2010).
[2] J. Shimoda, Y. Ohira, R. Yamazaki, J. M. Laming, and S. Katsuda, Mon. Not. R. Astron. Soc. **473**, 1394 (2017).
[3] K. Heng and R. A. Sunyaev, A&A **481**, 117 (2008).
[4] D. Tseliakhovich, C. M. Hirata, and K. Heng, Mon. Not. R. Astron. Soc. **422**, 2356 (2012).
[5] B. T. Draine, *Physics of the Interstellar and Intergalactic Medium* (Princeton University Press, New Jersey, 2010).
[6] K. Heng and R. McCray, Astrophys. J **654**, 923 (2007).
[7] I. B. Abdurakhmanov, A. S. Kadyrov, and I. Bray, J. Phys. B **49**, 03LT01 (2016).
[8] I. B. Abdurakhmanov, A. S. Kadyrov, S. K. Avazbaev, and I. Bray, J. Phys. B **49**, 115203 (2016).
[9] S. K. Avazbaev, A. S. Kadyrov, I. B. Abdurakhmanov, D. V. Fursa, and I. Bray, Phys. Rev. A **83**, 022710 (2016).

[10] I. B. Abdurakhmanov, A. S. Kadyrov, and I. Bray, Phys. Rev. A **94**, 022703 (2016).
[11] I. B. Abdurakhmanov, J. J. Bailey, A. S. Kadyrov, and I. Bray, Phys. Rev. A **97**, 032707 (2018).
[12] M. Keim, A. Werner, D. Hasselkamp, K.-H. Schartner, H. J. Lüdde, A. Achenbach, and T. Kirchner, J. Phys. B **38**, 4045 (2005).
[13] A. Donnelly, J. Geddes, and H. B. Gilbody, J. Phys. B **24**, 165 (1991).
[14] D. Detleffsen, M. Anton, A. Werner, and K. H. Schartner, J. Phys. B **27**, 4195 (1994).
[15] B. M. McLaughlin, T. G. Winter, and J. F. McCann, J. Phys. B **30**, 1043 (1997).
[16] T. G. Winter, Phys. Rev. A **80**, 032701 (2009).
[17] O. Marchuk, Y. Ralchenko, and D. R. Schultz, Plasma Phys. Control. Fusion **54**, 095010 (2012).
[18] I. B. Abdurakhmanov, S. U. Alladustov, J. J. Bailey, A. S. Kadyrov, and I. Bray, Plasma Phys. Control. Fusion **60**, 095009 (2018).
[19] M. Hughes, J. Geddes, R. McCullough, and H. Gilbody, Nucl. Instr. and Meth. B **79**, 50 (1993).
[20] J. T. Park, J. E. Aldag, J. M. George, and J. L. Peacher, Phys. Rev. A **14**, 608 (1976).
[21] D. Belkic, S. Saini, and H. S. Taylor, Phys. Rev. A **36**, 1601 (1987).
[22] R. F. Syms, M. R. C. McDowell, L. A. Morgan, and V. P. Myerscough, J. Phys. B **8**, 2817 (1975).
[23] A. Werner and K.-H. Schartner, J. Phys. B **29**, 125 (1996).
[24] F. Martin, J. Phys. B **32**, 501 (1999).
[25] D. R. Schultz and S. Y. Ovchinnikov, J. Phys. Conf. Ser. **576**, 012008 (2015).